Proceedings of the 2003 IEEE International Frequency Control Symposium and PDA Exhibition
Jointly with the 17th European Frequency and Time Forum

Endcaps for TE_{01} Cavities in Fountain Frequency Standards

N. Ashby[1], S. Römisch[2], S.R. Jefferts[3]

[1]University of Colorado
Department of Physics
Boulder, Colorado 80305

[2] Script L, LLC .
1212 Main St
Louisville, Colorado 80027

[3]Time and Frequency Division
National Institute of Standards and Technology
325 Broadway
Boulder, Colorado 80305

I. INTRODUCTION

The microwave cavity currently used universally for Ramsey interrogation in cesium fountain primary frequency standards is a cylindrical cavity running in the TE_{01} mode at 9.192 GHz [1,2,3]. The design of this type of cavity is relatively straightforward, but as fountain frequency standards have pushed to the 10^{-15} level of absolute frequency inaccuracy the details of the cavity design have become important. We look at three distinct problems in this paper related to the details of the design of the endcaps of the TE_{01} cavity. First, motivated by a paper by Gibble *et al*., at the 2002 IEEE Frequency Control Symposium we investigate analytically the fields within the cavity near the entrance and exit apertures of the cavity [4]. Some hitherto unsuspected effects are noted, principally previously unseen diffraction-like effects in the field at the aperture. In the second section of the paper we look at the effect of mis-centering on the below-cutoff waveguide through which atoms enter and leave the Ramsey cavity. Finally we investigate an alternative design for choke structures which suppresses the unwanted (TM_{11}) mode which is normally degenerate in frequency with the TE_{01} mode.

II. FIELDS NEAR THE ENDCAPS

Stimulated both by the PARCS (Primary Reference Clock in Space) project [5] and by the report in 2002 by Gibble et al. [4] of potentially large frequency shifts caused by field reversals in the neighborhood of the input/output below-cutoff waveguide structures in fountain Ramsey cavities we have developed an analytic solution to the microwave fields within a typical TE_{01} cavity as used in, for example NIST-F1 [6].

The analytic solution of the field within the cavity and below waveguide structure is straightforward to calculate [7]. Using the notation in Fig 1 as well as

$$\omega = 2\pi(9{,}192{,}631{,}770), \quad \lambda_n = \sqrt{\left(\frac{\rho_n}{a_2}\right)^2 - \left(\frac{\omega}{c}\right)^2}, \quad n = 1,2,..$$

$$k_1 = \sqrt{\left(\frac{\omega}{c}\right)^2 - \left(\frac{\rho_1}{a_1}\right)^2}, \quad k_n = \sqrt{\left(\frac{\rho_n}{a_1}\right)^2 - \left(\frac{\omega}{c}\right)^2}, \quad n = 2,3,....$$

the fields within the cavity (region II in Fig. 1) are written in terms of Bessel functions as

$$\vec{E} = C_+ \frac{dJ_0(\frac{\rho_1 r}{a_1})}{dr} e^{jk_1 z}\hat{\varphi} + C_- \frac{dJ_0(\frac{\rho_1 r}{a_1})}{dr} e^{-jk_1 z}\hat{\varphi} + \sum_2^\infty (C_n e^{k_n z} + D_n e^{-k_n z}) \frac{dJ_0(\frac{\rho_n r}{a_1})}{dr}\hat{\varphi}$$

$$j\omega\vec{B} = [C_+(-jk_1)e^{jk_1 z} + C_-(jk_1)e^{-jk_1 z}] \frac{dJ_0(\frac{\rho_1 r}{a_1})}{dr}\hat{r} + \sum_2^\infty (-k_n C_n e^{k_n z} + k_n D_n e^{-k_n z}) \frac{dJ_0(\frac{\rho_n r}{a_1})}{dr}\hat{r} + [\frac{\rho_1^2}{a_1^2}(C_+ e^{jk_1 z} + C_- e^{-jk_1 z}]J_0(\frac{\rho_n r}{a_1})\hat{z} + \sum_2^\infty -\frac{\rho_n^2}{a_1^2}[C_n e^{k_n z} + D_n e^{-k_n z}]J_0(\frac{\rho_n r}{a_1})\hat{z}$$

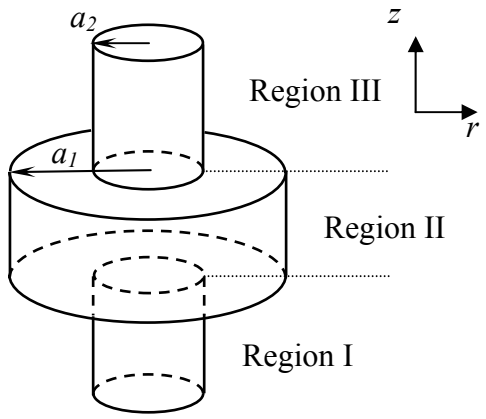

Figure 1. The microwave cavity with the relevant dimensions and features labeled.

The fields in the below-cutoff waveguide (Region I in Figure 1) can be written as

$$\vec{E} = \sum A_n \frac{dJ_0\left(\frac{\rho_n r}{a_2}\right)}{dr} e^{-\lambda_n z}\hat{\varphi} \quad \text{and}$$

$$j\omega\vec{B} = \sum A_n[-\frac{\rho_n^2}{a_2^2} J_0\left(\frac{\rho_n r}{a_2}\right)\hat{z} + \lambda_n \frac{dJ_0\left(\frac{\rho_n r}{a_2}\right)}{dr}\hat{r}]e^{-\lambda_n z} \ .$$

The fields in region III can be obtained from the fields in region I with the substitution of z→-z and by replacing the coefficients A_n with new coefficients B_n.

In the case of ideal conductive surfaces the boundary conditions on the conductor (where $\hat{n}$ is the unit normal vector to the surface) are as given in [7] $\vec{E}\times\hat{n} = 0$ and $\vec{B}\cdot\hat{n} = 0$.

The additional boundary condition which must be applied at the surface of the cavity where the below-cutoff waveguide enters can be stated as requiring that both E_φ and dE_φ/dz must be continuous across the boundary between region II and regions I and III.

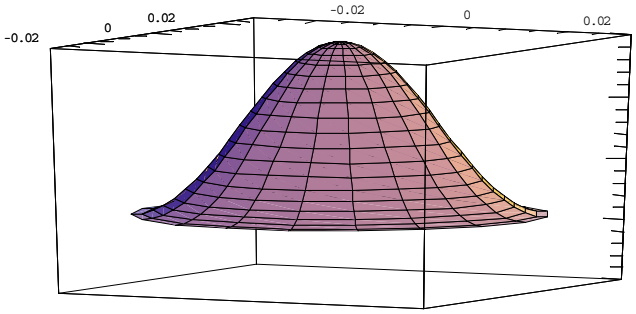

Figure 2. The microwave magnetic field at the mid-plane of the cavity. The field is normalized to unity at the center of the cavity. The units on the x and y axis are meters.

Applying these boundary conditions as well as symmetry conditions determines the expansion coefficients A_n, B_n, C_+, C_-, C_n, and D_n up to an overall factor (which can be thought of as the input microwave power).

Having now expanded the fields in a normal-mode solution we can sum the series involved and plot the fields within the cavity and waveguides. The cavity used in the model is 0.06 m in diameter and the length is approximately 0.022 m. The actual length is adjusted in the model to give a resonant frequency equal to the cesium hyperfine splitting (9.19263177 GHz).

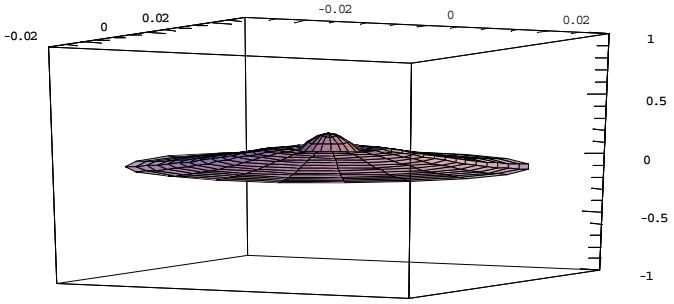

Figure 3. The microwave magnetic field 1mm above the endcap of the cavity, 90% of the distance from the center to the endcap. The field reversal is beginning to be visible at this point.

In Figure 2 we plot the magnetic field at the mid-plane of the cavity. The field here (far from the input/output waveguides) looks essentially like that we would expect from the solution of an isolated TE_{011} mode within the cavity. Figure 3 showing the field about 90% of the way to the endcap. This close to the below-cutoff waveguide the microwave field is still well behaved albeit beginning to show a field reversal. In Figure 4, the field at the endcap, plotted only over the input waveguide clearly shows the field structure caused by the below-cutoff waveguide.

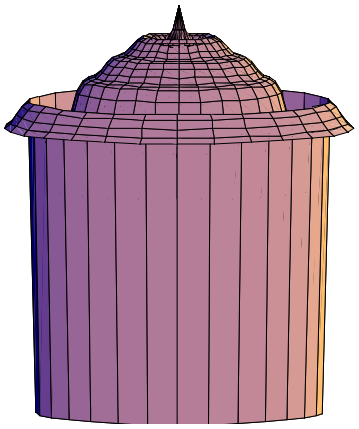

Figure 4. The field at the endcap of the microwave cavity plotted only over the below-cutoff waveguide (0<r<0.005m, z=L/2). The effect of the below-cutoff waveguide can be clearly seen as a large field reversal at this point. The diffraction rings can also be seen in the "staircase-like" behavior of the field strength.

An unexpected effect, which we believe is a diffraction effect from the sharp edges of the below-cutoff waveguide, can be seen in Figures 4 and 5. The quasi-periodic "wiggles" in the field between r=0 and the edge of the below-cutoff

waveguide at r = 0.005 m are evident in the field solutions both in the cavity and in the below-cutoff waveguide at z = L2/ ± ε. In Figure 5 both of these solutions are overlaid, the solution inside the cavity having 300 terms in the expansion and the solution inside the below-cutoff waveguide having 50 terms.

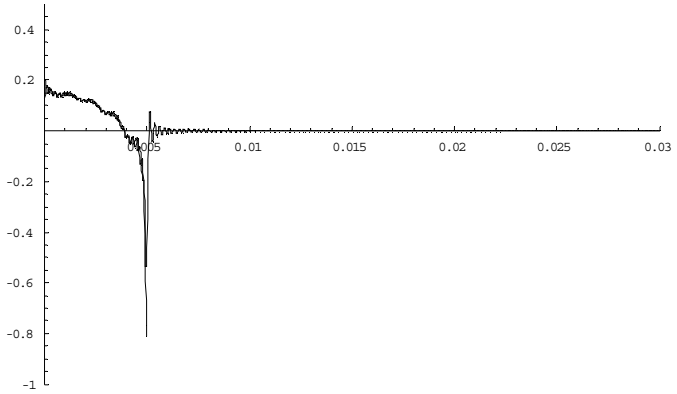

Figure 5. The field solutions just inside the below-cutoff waveguide and just inside the cavity (z = L/2 ± ε) are overlaid. The large overshoot of the solutions at the edge of the below-cutoff waveguide is a Gibbs phenomenon. The "diffraction" pattern caused by the below-cutoff waveguide edge can be seen in the four or five wiggles between r = 0 and r = 0.005 m.

The z component of the microwave magnetic field along the z-axis and near the edge of the below-cutoff waveguide is shown in Figures 6 and 7. The on-axis field is well behaved and shows no sign of field reversal, while the field near the waveguide shows a reversal, as seen in Figure 7.

Finally, in Figure 8, we show a plot of the microwave magnetic field within the cavity showing the penetration of the field into the below-cutoff waveguides.

It should be noted that no effects predicted by the model so far lead to a frequency shift. Reversals in the field lead to a small loss of contrast in the Ramsey fringe, not a frequency shift. The model presented here is not yet complete as losses in the walls are not taken into account. Losses lead to distributed cavity phase shifts, which can cause frequency shifts.

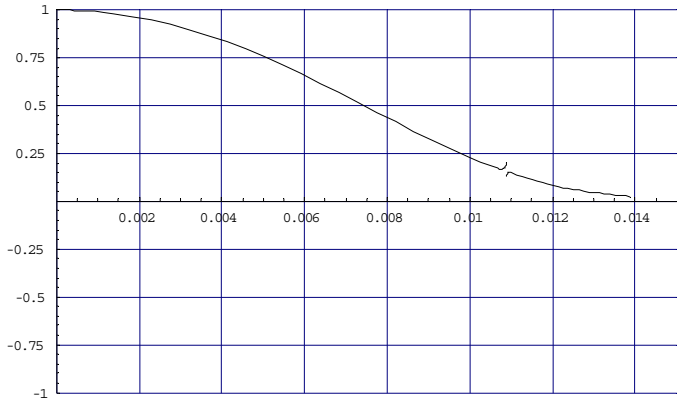

Figure 6. The on-axis (r = 0) z component of the microwave magnetic field plotted as a function of distance from the center of the cavity in the z direction. The small discontinuity in the field at z ~ 0.011 m is a result of the previously mentioned Gibbs phenomenon. The field strength is normalized to unity at the center of the cavity, r = 0, z = 0.

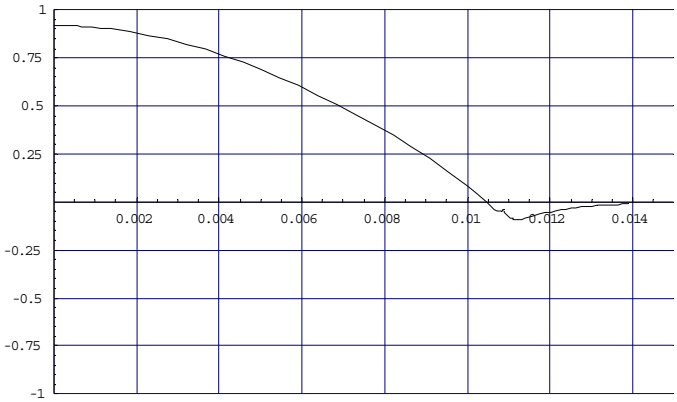

Figure 7. The z component of the microwave magnetic field plotted as a function of distance from the center of the cavity in the z direction at r = 0.0045 m (next to the edge of the below-cutoff waveguide). The small discontinuity in the field at z ~ 0.011 m is a result of the previously mentioned Gibbs phenomenon. The field strength is normalized to unity at the center of the cavity, r = 0, z = 0.

High-power microwave tests on atoms in several cesium fountain primary standards [1,2,3] lead directly to the conclusion that frequency shifts from these effects are, at most, in the range of $\delta f/f = 2\times10^{-16}$, not the $\delta f/f = 10^{-15}$ range suggested in [4].

III. EXCITATION OF THE TE_{11} MODE IN THE BELOW-CUTOFF WAVEGUIDE DUE TO MIS-CENTERING OF THE WAVEGUIDE IN THE CAVITY

The theoretical model presented so far, while powerful and general, is quite labor-intensive to use. We therefore adopt a simpler, less general and less precise method to evaluate two further endcap effects.

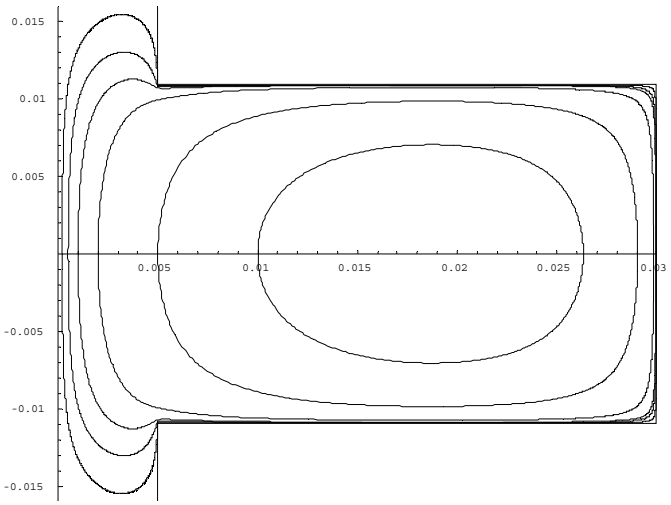

Figure 8. The pattern of the magnetic field within the cavity shown in an r-z plot. The units on the axis are meters. The density of field lines should not be taken as an indication of the field strength, as the lines plotted were simply chosen for clarity.

The first of these two problems concerns the below-cutoff waveguides that allow atoms to enter and leave the cavity. These waveguides are nominally centered in the cavity, but, due to unavoidable imperfections in the construction of the cavity, they are generally slightly mis-centered. If the waveguide is perfectly centered, the TE_{01} mode in the cavity excites only the TE_{01} mode in the waveguide. If on the other hand the waveguide is mis-centered the TE_{01} mode can also excite other modes in the below-cutoff waveguide, notably the dominant TE_{11} mode, leading to higher than expected leakage of the cavity field to the outside world.

We estimate the effect of mis-centering by noting that the normal modes of a waveguide provide an orthogonal set in which to expand an arbitrary field. If we denote the electric field associated with the j[th] mode of the waveguide by $\vec{E}_i$ and impose the normalization condition $\int \vec{E}_i \vec{E}_j^{*} dA = \delta_{ij}$ the electric field associated with the TE_{01} and TE_{11} modes can be written as

$$\vec{E}_{01} = \frac{-j\rho_{01}^{'}}{\sqrt{1.191*2\pi}} J_0^{'}\left(\frac{\rho_{01}^{'}\rho}{a_1}\right)\hat{\varphi} \quad \text{and}$$

$$\vec{E}_{11} = \frac{\rho_{11}^{'}}{a_2}\frac{j}{\sqrt{1.504*\pi}} J_1^{'}\left(\frac{\rho_{11}^{'}\rho}{a_2}\right)\cos\varphi\,\hat{\varphi}$$

where $\rho'_{n,m}$ is the m[th] zero of J'_n and a_1 and a_2 are respectively the radii of the cavity and below-cutoff waveguide. If we assume that the cavity is mis-centered with respect to the below-cutoff waveguide by a distance $\rho_m << a_1$ the coordinate ρ can simply be replaced by $\rho - \rho_m \cos\varphi$. We then expand J'_0 as

$$J_0^{'}(x) \cong -\frac{x}{2} + \frac{(x/2)^3}{1^2 2} - \frac{(x/2)^5}{1^2 2^2 3}\ldots$$

Keeping only the lowest order terms in ρ we obtain

$$\vec{E}_{01} \approx \left(\frac{\rho_{01}^{'}}{2a_1}\right)\left(\frac{j\rho_{01}^{'}}{a_1\sqrt{1.191*2\pi}}\right)(\rho - \rho_m\cos\varphi)\,\hat{\varphi}\,.$$

The electric field of the TE_{01} mode in the mis-centered cavity is now approximated in the coordinate system of the below-cutoff waveguide. The fractional excitation (FE_{11}) of the TE_{11} mode in this coordinate system is now given by the expression

$$FE_{11} \approx \frac{\int_{aperture} \vec{E}_{01_{cavity}} \cdot \vec{E}^{*}_{11_{waveguide}}\, da}{\int_{aperture} \vec{E}_{01_{cavity}} \cdot \vec{E}^{*}_{01_{waveguide}}\, da}$$

where the denominator is required for normalization. The denominator can be evaluated as being $\frac{5}{4}\left(\rho'_{01}\right)^2\left(\frac{a_2}{a_1}\right)^3$. The numerator can be written as

$$\int_{aperture}\left(\frac{\rho_{01}^{'}}{2a_1}\frac{j\rho_{01}^{'}}{a_1\sqrt{1.191*2\pi}}\frac{-j\rho_{11}^{'}}{a_2\sqrt{1.504\pi}}(\rho - \rho_m\cos\varphi)\right.$$
$$\left. J_1^{'}\left(\frac{\rho_{11}^{'}\rho}{a_2}\right)\cos\varphi\;\rho\,d\rho\,d\varphi\right),$$

which evaluates to $2\frac{a_2\rho_m}{a_1^2}$. The net result for the fractional excitation of the TE_{11} mode of the below-cutoff waveguide is $FE_{11} \cong \frac{8a_1\rho_m}{5a_2^2\left(\rho'_{01}\right)^2}$. In NIST-F1 the relevant dimensions are known, and the fractional excitation can be evaluated using $a_1 = 0.03$ m, $a_2 = 0.005$ m, $\rho_m \le 12.5$ μm ($\rho'_{01} = 3.832$). The fractional excitation of the TE_{11} mode, relative to the TE_{01} mode, is therefore about -56 dB (assuming the full 12.5μm mis-centering). The attenuation of the 1 cm diameter below-cutoff waveguide is 67 dB/cm at 9.192 GHz for the TE_{01} mode and only 32 dB/cm for the TE_{11} mode (See the appendix for a derivation of this result) . The below-cutoff waveguides in NIST-F1 are 10 cm long giving a theoretical attenuation of the cavity field by the TE_{01} mode of 670 dB, while if we assume a mis-centering of the below-cutoff waveguide of 12.5μm, the TE_{11} mode in the below-cutoff waveguide attenuates the field within the cavity by only 376 dB (320 dB + 56 dB). The TE_{11} mode is therefore likely to be the dominant source of leakage of the field within the microwave cavity even with tight construction tolerances.

IV. MODE-FILTER CHOKES FOR THE TM_{11} MODE

The TM_{111} mode is degenerate in frequency with the TE_{011} mode in a perfect cylindrical microwave cavity. The degeneracy occurs as a result of the property of Bessel functions that $J_1(x) = -\frac{dJ_0(x)}{dx}$. The TM_{111} mode, if excited, can cause frequency shifts in the fountain and is normally displaced in frequency through the use of mode-filter chokes in the endcap(s) of the cavity.

The operation of the chokes can be roughly understood by considering the surface currents on the cavity walls for the TE_{011} and TM_{111} modes. The surface currents of the TE_{011} mode are azimuthal in nature, running in concentric circles on the endcaps and cavity walls. The TM_{111} surface currents, on the other hand, originate on one endcap, run up the side-wall of the cavity and terminate on the other endcap. A gap between the endcap and sidewall of the cavity therefore has a minimal effect on the TE mode, while having a much larger

effect on the TM mode. We now analyze the construction of the gap (mode-filter choke) more rigorously.

A cylindrical microwave cavity can be seen as a length L_c of circular waveguide terminated with two ideal short-circuit plates (losses are neglected). Generally speaking it is possible to use a transmission-line equivalent circuit for each of the modes propagating in a waveguide, so that the analysis of a complex structure can be done using impedances, voltages and currents instead of EM fields. In this perspective, the same cylindrical cavity can be represented as a length of transmission line (representing the resonant mode) terminated with two short circuits, as shown in Figure 9, where Γ_1 and Γ_2 are the reflection coefficients.

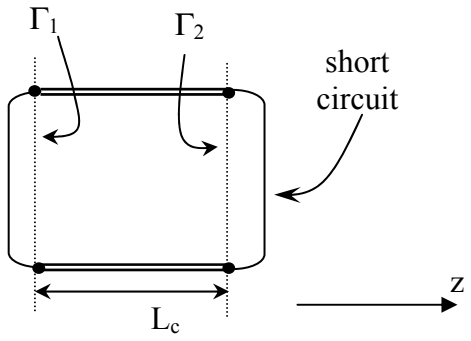

Figure 9. The microwave cavity modeled as a length of transmission-line terminated with two short circuits.

The resonance condition can then be written as

$$\Gamma_2\, e^{-j2k_c L_c}\, \Gamma_1 = 1\,,$$

where the frequency dependence of k_c allows the calculation of the resonance frequency. Because the reflection coefficient of a short circuit is equal to -1, the resonance frequency for the TE_{01} mode in a circular cavity of length L_c is:

$$e^{-j2k_c L_c} = 1 \;\rightarrow\; k_c = \frac{\pi}{L_c} \;\rightarrow\; \omega_0 = \sqrt{\frac{1}{\varepsilon\mu}\left(\frac{\pi^2}{L_c^2} - \frac{\left(\rho'_{01}\right)^2}{a_1^2}\right)}$$

where

$$k_c = \sqrt{\omega^2\varepsilon\mu - \left(\frac{\rho'_{01}}{a_1}\right)^2}$$

is the propagation constant (or wave number) for the TE_{01} mode in a circular waveguide.

The addition to the cavity of a choke in order to decouple the TM_{11} mode from the TE_{01} mode can be modeled as a length of coaxial waveguide (L_{choke}) added to one end of the cavity. The standard choke design is simply as shown in Figure 10. In our case the modes of interest in the cavity are the TM_{11} and TE_{01}, which will couple to the equivalent ones in the coaxial waveguide and to a number of other modes that have similar field patterns across the annular gap. In order to understand the effect of the choke on the cavity modes it is necessary to quantitatively evaluate the coupling to the different coaxial modes.

Table 1 lists the cutoff frequencies for the TE and TM coaxial modes in the case of a coaxial waveguide with a gap of 1 mm (typical of the dimensions used in fountain cavities) between the inner and outer conductor.

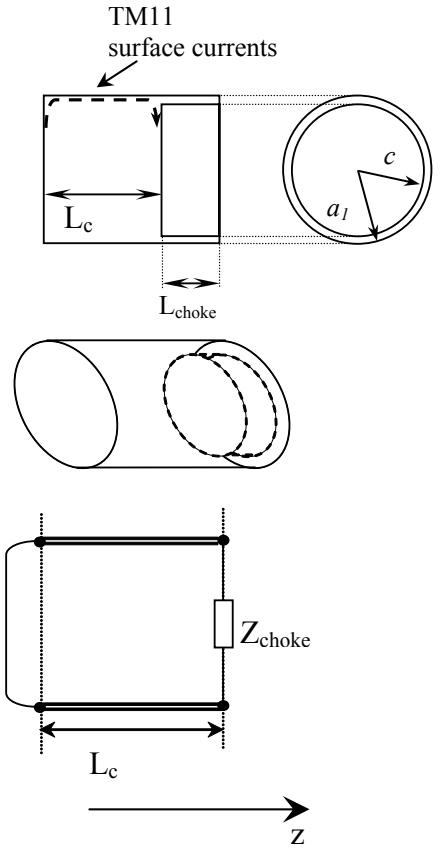

Figure 10. A traditional TM mode-filter choke is added to the microwave cavity.

n	TEn1	TMn1
0	74.95	74.816
1	1.638	74.833
2	3.290	74.883
3	4.929	74.966
4	6.580	75.082
5	8.203	75.230
6	9.857	75.410
7	11.519	75.622
8	13.156	75.864
9	14.785	76.135
10	16.456	76.435

Table 1. The cutoff frequencies of the coaxial waveguide mode filter choke (in GHz). Note that only the low order TE modes are propagating.

The only propagating modes inside the coaxial waveguide with a 1mm gap are: TE_{11}, TE_{21}, TE_{31}, TE_{41}, TE_{51}.

A quantitative estimate of the coupling strength for all the modes is given by the integral of the two modes over the annular gap:

$$overlap = \int_0^{2\pi}\int_c^a E_i \cdot E_j\, r dr d\theta$$

where *i* is the mode index in the cavity and *j* indicates the mode in the coaxial waveguide.

The coupling coefficients calculated as described above are listed in Table 2. The TE_{01} and TM_{11} coaxial modes are not propagating in the case of the small gap (1 mm), but their coupling coefficient is nonzero: the cavity modes will couple to the evanescent modes. The effect of coupling into an evanescent mode is a phase shift of the incident field, due to the reactive energy stored in the non-propagating mode. The coupling coefficients shown in Table 2 are each represented in the transmission-line equivalent circuit as a purely imaginary shunt impedance (reactance) at the discontinuity between the two transmission lines.

coax / circ	TE01	TM11	TE11	TEn1 n>1
TE01	$15\cdot10^{-3}$	0	0	0
TM11	0	$234\cdot10^{-3}$	$2\cdot10^{-3}$	0

Table 2. Coupling coefficients between modes when gap is 1mm. The TE_{01} and TM_{11} coaxial modes are not propagating with the small gap, so these are coupling coefficients into evanescent modes

The coupling coefficient is the field transmission coefficient from the circular waveguide to the coaxial waveguide, or equivalently the voltage transmission coefficient in the transmission-line equivalent circuit of Figure 11.

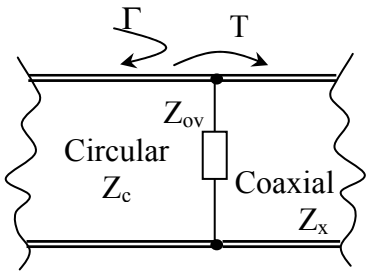

Figure 11. The model used of the junction between the coaxial waveguide (mode filter choke) and the cylindrical cavity.

The general expression for the transmission coefficient is

$$T = 1 + \Gamma = \frac{2Z_{ov}Z_{coax}}{Z_{coax}Z_{circ} + Z_{ov}(Z_{circ} + Z_{coax})}.$$

The coupling coefficient calculated with the overlap integral doesn't contain the phase information: it is only the modulus of T. Z_{ov} is purely imaginary and is capacitive or inductive, depending on the field geometry: capacitive for TM (also when coupling into the TE coax) and inductive for TE. The two cases when Z_{coax} is either real or imaginary (propagating modes in the coaxial waveguide as opposed to evanescent ones) need to be considered separately.

If Z_{coax} is real:

$$X_{ov} = \pm \frac{Z_{coax}Z_{circ}|T|}{\sqrt{4Z_{coax}^2 - |T|^2 (Z_{coax} + Z_{circ})^2}},$$

where $Z_{ov} = jX_{ov}$

while if Z_{coax} is imaginary:

$$X_{ov} = X_{coax}Z_{circ}|T| \frac{-Z_{circ}|T| \pm X_{coax}\sqrt{4 - |T|^2}}{\left(X_{coax}^2 + Z_{circ}^2\right)|T|^2 - 4X_{coax}^2}.$$

where $Z_{ov} = jX_{ov}$ and $Z_{coax} = jX_{coax}$

The characteristic impedance of each mode in both circular and coaxial waveguides is given in Table 3 (Ohms) and the complete equivalent circuits for the cavity modes loaded by the choke are shown in Figure 12.

Circ		Coax						
TE01	**TM11**	**TE01**	**TM11**	**TE11**	**TE21**	**TE31**	**TE41**	**TE51**
282	282	-j23	j6131	382	402	443	529	777

Table 3. Impedances of the propagating modes in circular and coaxial (except for TE01 and TM11 coax, they are not propagating) for the case with a 1-mm gap (inner conductor radius c = 0.029 m) .

The TE_{01} mode in the cavity is loaded with the reactive characteristic impedance of the evanescent TE_{01} coaxial mode (represented by a capacitor), via the coupling coefficient evaluated by the overlap integral. In Figure 12 the coupling coefficient is represented by the impedance Z_{ov}.

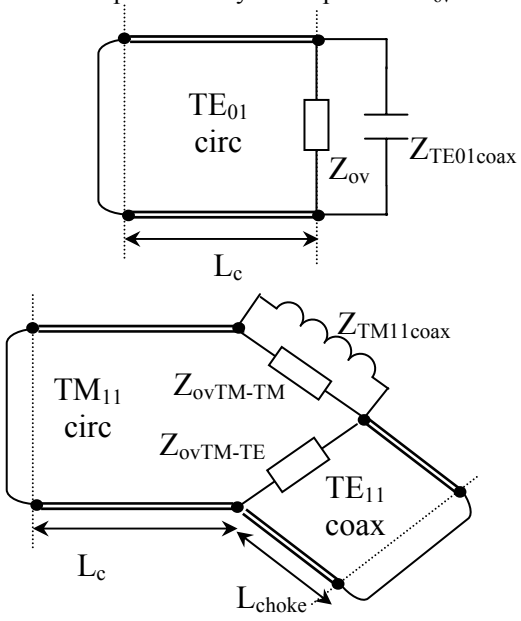

Figure 12. Transmission-line equivalent circuits for TE_{01} (top) and TM_{11} (bottom) modes inside the cavity, when loaded with a simple choke with a 1mm-annular gap.

The TM_{11} mode in the cavity couples with the TE_{11} coaxial propagating mode and with the TM_{11} coaxial evanescent mode. The two modes are represented by two separate loads connected in series. In fact the transmission-line equivalent circuit for multimode waveguides is a multiport network, with one port per mode.

The resonant condition for the circuits in Figure 12 is:

$$\Gamma_2 \, e^{-j2k_c L_c} \, \Gamma_1 = 1$$

where, for the TE_{01} mode

$$\Gamma_1 = \frac{Z_{tot} - Z_{TE01circ}}{Z_{tot} + Z_{TE01circ}} \quad \text{and} \quad Z_{tot} = Z_{ov} \,//\, Z_{TE01coax}$$

while for the TM_{11} mode

$$\Gamma_1 = \frac{Z_{tot} - Z_{TM11circ}}{Z_{tot} + Z_{TM11circ}} \quad \text{and}$$

$$Z_{tot} = \left(Z_{ovTM-TM} \,//\, Z_{TM11coax}\right) + \left(Z_{ovTM-TE} \,//\, jZ_{TE11coax} \tan\left(\beta_{TE11coax} L_{choke}\right)\right).$$

The two modes are loaded differently by the choke. The new resonant frequencies are calculated from the modified resonance condition. The differences with respect to the resonance of the cavity without a choke (assumed to be 9.192 GHz) are shown in Table 4.

TE01	TM11
-11.5 MHz	-196 MHz

Table 4. Displacement of the resonance frequency due to the loading by simple choke with an annular gap of 1mm.

These calculated frequency offsets are typical of those observed in properly constructed copper cavities used in Cs fountain primary standards.

Because the only propagating mode in the coaxial waveguide is the TE_{11} mode, the effect of its coupling with the TM_{11} mode in the cavity is dependent on the length of the choke. Given at least a certain length of choke (L_{choke} □ characteristic attenuation length), the coupling to the evanescent mode is independent of choke length. Therefore, the displacement of the TM_{111} resonance frequency is almost independent of the choke length because the coupling coefficient between the TM_{11} mode in the cavity and the TM_{11} coaxial mode is much larger then the one between the TM_{11} cavity mode and TE_{11} coaxial mode. The dominant effect therefore is given by the coupling with the evanescent TM_{11} coaxial mode.

V. NEW CHOKE: DIAPHRAGM WITH 1 MM GAP AND COAXIAL WAVEGUIDE WITH 12 MM INNER CONDUCTOR RADIUS.

In order to allow propagation of the TM_{11} mode inside the coaxial waveguide and to try to improve the coupling with the TM11 mode in the cavity, it is necessary to increase the gap, reducing the radius of the inner conductor of the coaxial waveguide. However, the simple choke design with such increased gap is not usable because will heavily affect the TE_{01} mode in the cavity. For this reason a thin diaphragm with a small annular gap of 1mm is used between the coaxial waveguide and the circular waveguide, as shown in Figure 13.

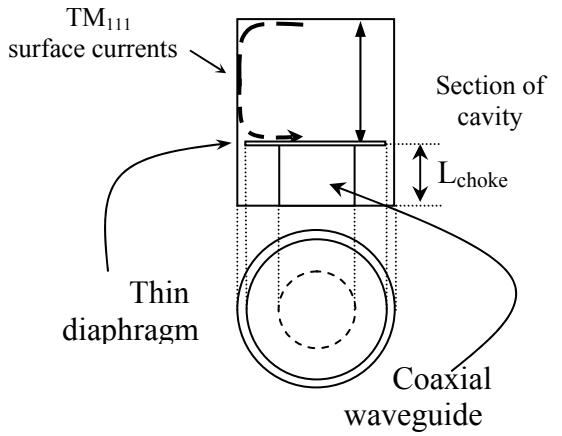

Figure 13. New design of the choke for the cylindrical cavity using a coaxial waveguide with reduced inner conductor radius and a thin diaphragm with a smaller annular gap placed between the cavity and the coaxial waveguide.

While this design works to greatly increase the displacement of the TM_{111} mode in the cavity, unfortunately, the TE_{01} mode in the coaxial waveguide is also propagating. This results in a small real impedance being imposed upon the TE_{01} mode in the cavity. This real impedance implies power flow within the cavity with the obvious resulting concerns regarding the distributed cavity phase shifts, both transverse and longitudinal. We are continuing to investigate this structure and will report results when they become available.

ACKNOWLEDGEMENTS

We are pleased to acknowledge helpful conversations with Andrea DeMarchi, Bill Klipstein, Eric Burt and Tom Parker. John Dick has been especially helpful pointing out the cross mode (TM to TE) coupling possibility as well as generally elucidating several points.

APPENDIX- ATTENUATION IN BELOW-CUTOFF CIRCULAR WAVEGUIDES

The following result is useful in the evaluation of the attenuation of the below-cutoff circular waveguides used in the fountain cavities we have been discussing in this paper.

The electric field in a waveguide can be written $E = E_0 e^{j(\omega t - kz)}$. If the time dependence is eliminated we have $E = E_0 e^{-jkz}$, where $k = \frac{2\pi}{\lambda_0}\sqrt{1-(\lambda_0/\lambda_c)^2}$. Using standard notation, λ_0 is the free space wavelength, ($\lambda_o = \frac{c}{\nu}$), and λ_c is the cutoff wavelength for the particular mode in

question in the waveguide. In circular waveguide λ_c can be written [7],

$$TE_{m,n}: \quad \lambda_C = \frac{2\pi a}{\rho'_{m,n}}$$

$$\mathrm{TM_{m,n}}: \quad \lambda_C = \frac{2\pi a}{\rho_{m,n}},$$

where a is the radius of the waveguide, $\rho_{m,n}$ is the m^{th} zero of J_n, and $\rho'_{m,n}$ is the m^{th} zero of J'_n.
We therefore have

$$\frac{E}{E_0} = e^{-j\frac{2\pi z}{\lambda_0}\left[1-(\lambda_0/\lambda_c)^2\right]^{1/2}}$$

.If $\lambda_0 > \lambda_c$ (beyond cutoff) this can be rearranged as

$$\frac{E}{E_0} = e^{-\frac{2\pi z}{\lambda_c}\left[1-(\lambda_c/\lambda_0)^2\right]^{1/2}}.$$

Using the expression for λ_C in the TE case we can write the E/E_0 expression above as

$$\frac{E}{E_0} = e^{-\rho'_{n,m}\frac{z}{a}\left[1-(\lambda_c/\lambda_0)^2\right]^{1/2}}.$$

Finally, this can be converted to decibels to give:

$$Attenuation = 20 * Log(e) * \left(\rho'_{n,m}\frac{z}{a}\sqrt{1-\left(\frac{\lambda_c}{\lambda_0}\right)^2}\right)\left[dB/length\right].$$

The formula for the TM modes can be obtained with the substitution of $\rho_{n,m}$ for $\rho'_{n,m}$. The explicit forms for the low order modes are

$$TE_{11}: \quad \frac{16}{a}\sqrt{1-\left(\frac{3.42a}{\lambda_0}\right)^2} \text{ dB/ unit length}$$

$$TM_{01}: \quad \frac{20.9}{a}\sqrt{1-\left(\frac{2.61a}{\lambda_0}\right)^2} \text{ dB/ unit length}$$

$$TE_{01}: \quad \frac{33.3}{a}\sqrt{1-\left(\frac{1.64a}{\lambda_0}\right)^2} \text{ dB/ unit length}$$

REFERENCES

[1] S.R. Jefferts, J.H. Shirley, T.E. Parker, T.P. Heavner, D.M. Meekhof, C.W. Nelson, F. Levi, G. Costanzo, A. DeMarchi, R.E. Drullinger, L. Hollberg, W.D. Lee, and F.L. Walls, *Accuracy Evaluation of NIST-F1,* Metrologia **39** (321-336) Jan 2002.

[2] Roland Schroder, Udo Hubner, and Dieter Griebsch, *Design and Realization of the Microwave Cavity in the PTB Caesium Fountain Atomic Clock CS-F,* Transactions of the IEEE Ultrasonics, Ferroelectrics and Frequency Control (2002).

[3] Clairon A., et. al., in *Proc. 5th International Symposium of Frequency Standards and Metrology,* World Scientific (1996) pp49-59.

[4]Chad Fertig, Ruoxin Li, J. Irfon Rees and Kurt Gibble, *Distributed Cavity Phase and Microwave Photon Recoils*, 2002 IEEE Frequency Control Symposium, pp 469-472.

[5] T.P. Heavner, L. Hollberg, S.R. Jefferts, H.G. Robinson, D.B. Sullivan, F.L. Walls, N. Ashby, W. Klipstein, L. Maleki, D. Seidel, R. Thompson, S. Wu, L. Young, E. Mattison, R. Vessot, and A. DeMarchi, *PARCS, A Laser-Cooled Atomic Clock in Space,* Proc. 2001 Freq. Stand. Metrology Symp pp 253-260.

[6] S.R. Jefferts, R.E. Drullinger, and A. DeMarchi, *Cesium Fountain Microwave Cavities,* Proc. 1998 IEEE Intl. Freq. Cont. Symp., pp6-8.

[7] J.D. Jackson, *Classical Electrodynamics*, John Wiley and Sons (1975) 2nd edition.